Single-molecule live-cell imaging reveals parallel pathways of prokaryotic nucleotide excision repair

Harshad Ghodke[1,2*], Han Ngoc Ho[1,2], Antoine M van Oijen[1,2]

[1]Molecular Horizons and School of Chemistry and Molecular Bioscience, University of Wollongong, Wollongong, Australia

[2] Illawarra Health and Medical Research Institute, Wollongong, Australia

Abstract:

In the model organism *Escherichia coli,* helix distorting lesions are recognized by the UvrAB damage surveillance complex in the global genomic nucleotide excision repair pathway (GGR). Alternately, RNA polymerases stalled or paused by lesions signal the presence of DNA damage in transcription-coupled nucleotide excision repair (TCR). Ultimately, damage recognition is mediated by UvrA, culminating in the loading of the damage verification enzyme UvrB. We set out to characterize the differences in the kinetics of damage recognition by UvrA complexes formed during GGR and TCR. We followed functional, fluorescently tagged UvrA molecules in live cells and measured their residence times in TCR-deficient or wild-type cells. We demonstrate that the lifetimes of UvrA in Mfd-dependent or Mfd-independent repair are similar in live cells, and are governed by UvrB. Here, we illustrate a non-perturbative, imaging-based approach to quantify the kinetic signatures of damage recognition enzymes participating in multiple pathways in cells.

Across the various domains of life, the recognition and repair of bulky helix distorting lesions in chromosomal DNA is coordinated by nucleotide excision repair (NER) factors. Damage detection occurs in two stages: a dedicated set of damage surveillance enzymes (reviewed in ref.[1, 2, 3]) (namely the prokaryotic UvrA, and the eukaryotic UV-DDB, XPC, XPA and homologs) constantly survey genomic DNA for lesions. Upon DNA damage recognition, these enzymes load specific factors (UvrB in prokaryotes, TFIIH and homologs in eukaryotes) that unwind the DNA and verify the location of the damage with nucleotide resolution (Fig. 1a) (reviewed in ref.[2, 3]). Subsequently, specialized endonucleases (prokaryotic UvrC and homologs, and the eukaryotic XPF/XPG and homologs) are recruited to the site of the DNA, resulting in cleavage of the single-stranded DNA (ssDNA) patch containing the lesion (reviewed in ref.[2, 3]).

In all studied organisms, the recognition of DNA damage also occurs via the stalling of RNA polymerase at sites of lesions (reviewed in ref.[4]). In this case, a transcription elongation complex that is unable to catalyse RNA primer extension manifests as an ultra-stable protein-DNA roadblock. Transcription-repair coupling factors such as the prokaryotic Mfd, and the eukaryotic homologs Rad26/CSB are dedicated factors that recognize these TECs and remodel them[5, 6, 7, 8, 9]. In prokaryotes, Mfd is recruited to the site of a failed TEC, and in turn it recruits the UvrA(B) protein (Fig. 1) [7, 9, 10, 11]. Similarly, in eukaryotes, CSB is recruited to the site of a stalled RNAPII complex, and recruits the TFIIH complex[12].

Damage detection via elongating RNA polymerase is termed transcription-coupled repair (TCR), in contrast to the direct detection of lesions by the UvrAB damage sensor (global genomic repair, or GGR). Studies investigating the rate of repair during TCR vs. GGR, have reported an enhancement in the rate of removal of UV-induced lesions from the template strand in transcribed DNA compared to non-transcribed DNA[13, 14, 15, 16, 17, 18]. This observation has sparked several studies targeted at understanding the mechanistic basis of rate enhancement[11, 19, 20]. A recent single-molecule *in vitro* study reported that the time to incision in TCR is approximately four-fold faster than in GGR under certain conditions [11].

A diverse set of intermediates is readily formed *in vitro* - ranging from a translocating RNAP-Mfd complex, arrested RNAP-Mfd-$UvrA_2$ and the complete Mfd-$UvrA_2$-UvrB handoff complex in the presence of both UvrA and UvrB[10, 11]. To understand which of these intermediates are formed inside cells, we have recently visualized Mfd in cells and quantified its lifetime in the TCR reaction in cells[10]. A recent study failed to detect an influence of Mfd on the behaviour of UvrA in living cells[21]. Therefore, *in vitro* studies notwithstanding, how TCR is orchestrated by UvrA in cells remains unclear.

In this work, we revisited this question in the context of live cells and applied high-resolution single-molecule imaging methods that permit accurate measurements of DNA binding lifetimes over a broad timescale ranging from a few hundred milliseconds to several minutes[10, 22]. We asked the question: what is the lifetime of UvrA in TCR, compared to GGR? To answer this question, we visualized fluorescently tagged UvrA in cells and measured the lifetimes of the interactions with DNA in wild-type and TCR-deficient cells. We found that UvrA is long lived on DNA in the absence of UvrB and Mfd, and that its dissociation is promoted by UvrB in cells executing GGR. The cellular concentration of UvrA relative to UvrB strongly influenced its binding lifetime in interactions with DNA-bound Mfd during TCR. The kinetics of UvrA in TCR could only be detected under conditions of limiting UvrB, suggesting a role for UvrB in resolving Mfd-UvrA intermediates involved in TCR. Exposure to ultraviolet light (UV) led to an increase in the binding lifetime of UvrA in TCR-deficient cells. In contrast, in TCR-proficient cells, the DNA-bound lifetimes of UvrA and Mfd were identical, and dropped upon UV exposure. Together, these studies characterize the interaction of UvrA with Mfd in live cells. Here, we establish a comprehensive framework for characterizing the binding kinetics of DNA repair proteins participating in multiple parallel pathways *in vivo* using non-perturbative single-molecule imaging approaches.

RESULTS

Imaging of UvrA-YPet

To visualize the binding of UvrA to DNA in cells, we created a C-terminal fusion of UvrA to the yellow fluorescent protein (YPet[23]) at the native chromosomal locus of MG1655 cells using λ Red recombination (Fig. 2a)[10, 24]. This strategy enabled observation of fluorescent UvrA expressed from its native, SOS inducible promoter (Supplementary Movie 1). We first performed UV-survival assays to assess the ability of UvrA-YPet to execute nucleotide excision repair (NER). Compared to wild-type cells, *uvrA-YPet* cells exhibited somewhat poorer survival upon exposure to UV (Supplementary Fig. 1a). Considering that C-terminal fusions of UvrA are fully functional in NER[21, 25], this modestly lower survival of *uvrA-YPet* cells may be attributable to a lower efficiency of protein translation.

Therefore, we set out to measure the copy numbers of UvrA-YPet in *uvrA-YPet* cells grown in EZ-rich defined media supplemented with glucose at 30°C. Exponentially growing cells were deposited on a modified glass coverslip at the bottom of a flow cell and visualized by illumination with 514-nm laser light under continuous flow of growth medium (Fig. 2b). Images of *uvrA-YPet* cells revealed DNA-bound UvrA-YPet molecules that manifested as static foci and diffusive molecules contributing to

cellular background fluorescence (Fig. 2c). These observations are consistent with its role as a damage surveillance protein.

Exposure to laser light led to rapid loss of YPet signal due to photodarkening and photobleaching of the chromophore (Supplementary Movie 1). We used this loss of signal to measure copy numbers of UvrA-YPet in cells. Dividing the corrected cellular fluorescence intensity by the intensity of a single YPet molecule revealed a copy number of 16 ± 4 copies of UvrA-YPet per cell (Supplementary Fig. 1b-d). Copy numbers of UvrA-YPet are strongly influenced by the carbon source present in the growth medium, ranging from 9-43 copies (minimal media) to 129 copies (rich media) per cell [26]. These estimates exceed the copy numbers of UvrA-YPet detected in the *uvrA-YPet* strain grown in rich medium. The lower copy numbers of UvrA-YPet are consistent with the minor deficiencies in survival observed after UV exposure (Supplementary Fig. 1a).

Interval imaging strategy to measure DNA binding kinetics

Continuous imaging of UvrA-YPet could not be used to measure DNA binding lifetimes, since the apparent lifetime of a focus represents UvrA-YPet molecules dissociating from the site as well as bound UvrA-YPet molecules that are photobleached during the imaging. Consequently, measurement of interactions that last longer than the photobleaching lifetime is impossible. Instead we imaged UvrA-YPet using an interval imaging strategy[10, 22, 27, 28] (Fig. 2d) that elegantly deconvolutes the lifetime of the interaction of UvrA-YPet with DNA and the lifetime of the fluorescent probe. Briefly, the introduction of a dark interval (τ_d) between consecutive frames extends the observation time window. By acquiring the same number of frames in each video collected with a different dark interval, the photobleaching rate is maintained constant while the observation window is extended arbitrarily. From these videos, cumulative residence time distributions of DNA-bound UvrA-YPet are constructed. Since these distributions reflect a mixture of two populations (UvrA molecules that dissociate and YPet molecules that photobleached), fitting them to a sum of exponential functions permits extraction of the true off rate (k_{off}) and the photobleaching rate (k_b). This interval imaging strategy enables accurate quantification of binding lifetimes of UvrA-YPet over three orders of magnitude from 0.1 s to several minutes.

UvrA is long-lived on DNA in the absence of UvrB and Mfd

First, we interrogated UvrA binding kinetics in the absence of its two major interacting partners UvrB and Mfd. To that end, we transformed cells lacking UvrA, UvrB and Mfd with a low copy plasmid (pSC101, 3-4 copies/cell[29]) expressing the C-terminal YPet fusion of UvrA under its native promoter (pUvrA-YPet). In this case, the copy number of UvrA-YPet was found to be 120 ± 28 copies per cell

(Supplementary Fig. 1b-d). In cells lacking UvrB and Mfd (Δ*uvrA* Δ*uvrB* Δ*mfd*/ pUvrA-YPet), we expected that interactions of UvrA-YPet with chromosomal DNA would reflect two of its key activities: binding to non-damaged DNA and binding to endogenous DNA damage produced as a by-product of cellular metabolism (Fig. 3a). Indeed, measurements of UvrA-YPet kinetics of dissociation in these cells revealed two lifetimes that are an order of magnitude apart - a fast lifetime ($\tau_{\text{UvrA}|\Delta uvrA\ \Delta uvrB\ \Delta mfd\ ,\ \text{fast}}$) of 1.6 ± 0.1 s (72 ± 2 %) and a slow lifetime ($\tau_{\text{UvrA}|\Delta uvrA\ \Delta uvrB\ \Delta mfd,\ \text{slow}}$) of 24 ± 1 s (28 ± 2 %) (summarized in Fig. 3c; Supplementary Fig. 2a-b).To confirm this result, we also measured the binding lifetime of an mutant UvrA that is deficient in its interactions with UvrB and Mfd (Fig. 3b). Since UvrA interacts with both UvrB and Mfd via the interface formed by residues 131-250 [30, 31, 32], we expected that the labelled mutant UvrA lacking residues 131-250, UvrA(Δ131-250)-YPet, would be a faithful reporter of binding of kinetics of UvrA alone in *uvrB*$^+$ *mfd*$^+$ cells (Fig. 3b). Indeed, interval imaging of UvrA(Δ131-250)-YPet expressed from a low-copy plasmid (pUvrA(Δ131-250)-YPet) in Δ*uvrA* cells produced a binding lifetime ($\tau_{\text{UvrA}(\Delta 131-250)}$) of 29.7 ± 0.8 s (summarized in Fig. 3c, Supplementary Fig. 2c-d). Together, these results demonstrate that UvrA-YPet by itself is long lived on DNA. Notably, the lifetimes measured in our experiments reveal values that are larger than previous *in vitro* measurements of UvrA binding[25]. The presence of two binding lifetimes suggests two populations of UvrA on DNA potentially reflecting interactions with non-damaged DNA and damaged DNA.

Loading of UvrB promotes the dissociation of UvrA in GGR

Next, we studied the influence of UvrB on the DNA binding lifetime of UvrA in cells lacking the transcription-coupled repair pathway (*uvrA-YPet* Δ*mfd* cells; Fig. 3d). In these cells, UvrA-YPet dissociated with a fast lifetime ($\tau_{\text{UvrA}|\ \Delta mfd,\ \text{fast}}$) of 1.5 ± 0.1 s (amplitude: 78 ± 2%) and a slow lifetime ($\tau_{\text{UvrA}|\ \Delta mfd,\ \text{slow}}$) of 8.7 ± 0.4 s (22 ± 2%) (summarized in Fig. 3f; Supplementary Fig. 2e-f). The lifetime of the slowly dissociating species observed in our measurements matches the lifetime detected for the dissociation of UvrA in the presence of UvrB previously (7 s) [25]. Notably, the fast lifetime is consistent with measurements from a previous study[21]; however, in this study a long-lived population of UvrA was not detected in the absence of DNA damage[21].

Several *in vitro* studies have revealed that damage detection during NER proceeds via the loading of UvrB on DNA, followed by damage verification mediated *via* the helicase activity of UvrB [33, 34, 35]. To confirm that the measured lifetimes indeed correspond to loading of UvrB, as opposed to a stochastic dissociation of UvrA from DNA, we measured the lifetime of UvrA-YPet in *uvrA-YPet mfd*$^-$ cells expressing the β-hairpin deletion mutant of UvrB from the native *uvrB* locus (Methods). This mutant, UvrB(ΔβHG), is inefficiently loaded on DNA [36]. The lifetime ($\tau_{\text{UvrA}|\ uvrB(\Delta\beta HG)\ \Delta mfd}$) of UvrA-YPet in cells expressing UvrB(ΔβHG) from the chromosome was 148 ± 36 s (100%); over 15-fold longer than that

of UvrA-YPet in cells lacking Mfd (Fig. 3e-f, Supplementary Fig. 2g-h). These data indicate that the UvrA-UvrB($\Delta\beta$HG) complex is arrested on DNA.

The lack of a short-lived species of UvrA in cells expressing mutant UvrB implies that the detectable population of UvrA can be sequestered to the chromosome in the form of a long-lived complex. Such a complex has been detected in *in vitro* single-molecule DNA stretching assays that have demonstrated that UvrAB can slide on DNA [25]. Additionally, it follows that in wild-type cells, loading of UvrB on DNA must promote the dissociation of UvrA. Indeed, our single-molecule live-cell imaging results highlight the physiological relevance of models constructed from *in vitro* studies that demonstrate that UvrB facilitates the dissociation of UvrA from DNA [36, 37, 38]. These findings lead us to suggest that the 8.7s lifetime measured here corresponds to the lifetime of UvrA engaged in GGR at sites of endogenous DNA damage, where UvrA is turned over by UvrB loading.

The lifetime of UvrA in TCR is longer than that in GGR

We next set out to measure the residence time of DNA-bound UvrA in TCR in the absence of exogenous DNA damage. During this reaction, UvrA is recruited to DNA via Mfd to form the asymmetric handoff complex Mfd-$UvrA_2$-UvrB, unlike the symmetric UvrB-$UvrA_2$-UvrB complex formed during GGR (Fig. 1). Our previous characterization of Mfd demonstrated that the residence time of Mfd is governed by UvrA, indicating that UvrA is recruited to Mfd during normal growth[10]. Hence, we anticipated three scenarios for the lifetime of UvrA in wild-type cells. First, if the residence time of UvrA-YPet is equal to 8.7 s, this would indicate either that the lifetime of UvrA-YPet in TCR and GGR are similar, or that the lifetimes are different but the recruitment of UvrAB to RNAP-bound Mfd occurs so infrequently that only GGR complexes of UvrA are detected. Second, a lifetime shorter than 8.7 s would suggest that Mfd promotes the dissociation of UvrA. Finally, a lifetime longer than 8.7 s would indicate that Mfd stabilizes UvrA in the handoff complex.

To distinguish between these three scenarios, we imaged UvrA-YPet in wild-type cells. Interval imaging of UvrA-YPet revealed a short-lived species with a lifetime ($\tau_{UvrA,\,fast}$) of 1.9 ± 0.2 s (79 ± 0.2%) and a long-lived species of UvrA with a lifetime ($\tau_{UvrA,\,slow}$) of 12.0 ± 0.8 s (21 ± 2%) (Fig. 4a, Supplementary Fig. 3a-b). To identify whether this lifetime reflected interactions in GGR or TCR, we imaged *uvrA-YPet* cells in conditions where TCR is abolished by upon rifampicin (rif) treatment. Interval imaging of UvrA-YPet in rif-treated cells revealed a short-lived species with a lifetime ($\tau_{UvrA|rif,fast}$) of 1.5 ± 0.3 s (63 ± 3 %) and a long-lived species of UvrA-YPet possessing a lifetime ($\tau_{UvrA|rif,\,slow}$) of 9.6 ± 0.6 s (37 ± 3 %) (Fig. 4a, Supplementary Fig. 3c-d). As expected, the slow lifetime of UvrA-YPet in rif-treated cells matches that in cells lacking Mfd. The decrease in the long-lived lifetime from 12.0 s to 9.6 s indicates that a

slowly dissociating species of UvrA is lost upon rif treatment, one that is involved in Mfd-dependent TCR. From these results and our previous observations that the lifetime of Mfd is longer in cells lacking UvrA[10], we conclude that UvrA interacts with Mfd in live cells. Notably, its lifetime in TCR is longer than that in GGR.

The amount of UvrA relative to UvrB determines its lifetime in TCR

Since no mutants of UvrA have been identified that exclusively mediate TCR, we were limited in our ability to achieve experimental conditions under which only the TCR reaction may be observed in cells. Nevertheless, we hypothesized that the equilibrium between TCR and GGR in growing cells could be tipped at higher cellular concentrations of UvrA. We tested this hypothesis by measuring the lifetime of UvrA-YPet in wild-type cells expressing UvrA-YPet from the plasmid (Δ*uvrA*/pUvrA-YPet, see Supplementary Fig. 1b-d). The data revealed a short-lived species with a lifetime ($\tau_{UvrA|\uparrow, fast}$) of 2.0 ± 0.1 s (74 ± 2 %) and a previously unencountered population of long-lived UvrA possessing a lifetime ($\tau_{UvrA|\uparrow, slow}$) of 19 ± 1 s (26 ± 2%) (Fig. 4a, Supplementary Fig. 3e-f).

In cells, UvrA is involved in target search (24 ± 1 s lifetime, Fig. 3c) and damage recognition as part of $UvrA_2B_2$ (8.7 s lifetime, Fig. 3f) in addition to Mfd-dependent UvrA(B) complexes (with lifetime of at least 12 s). To identify whether this long-lived UvrA species (19 ± 1 s lifetime) interacts with Mfd, we treated Δ*uvrA/*pUvrA-YPet cells with rifampicin. Under this condition, we expected to recover the lifetime of UvrA in GGR i.e. $UvrA_2$ or $UvrA_2B_2$ complexes. Indeed, measurements of lifetimes of UvrA-YPet in rif-treated Δ*uvrA/*pUvrA-YPet cells revealed a lifetime ($\tau_{UvrA|\uparrow rif, slow}$) of 11.5 ± 0.6 s (25 ± 2%) and a short lifetime ($\tau_{UvrA|\uparrow rif, fast}$) of 1.7 ± 0.1 s (75 ± 2%) (Fig. 4a, Supplementary Fig. 3g-h). The faster turnover of UvrA in response to rif treatment reinforces the conclusion that the lifetime of UvrA in TCR is longer than that in GGR.

Notably, rif treatment of Δ*uvrA/*pUvrA-YPet cells yielded a lifetime (11.5 s) that is longer than that measured for rif-treated *uvrA-YPet* cells (9.6 s), and cells lacking *mfd* (8.7 s). The simplest explanation for this slightly longer lifetime is that under conditions of high relative UvrA/UvrB abundance the population is composed of $UvrA_2B_{(2)}$ complexes (GGR) and DNA-bound $UvrA_2$ awaiting turnover by UvrB. The finding that UvrA and UvrB rarely co-diffuse in solution supports this model[21]. At higher cellular concentrations of UvrA relative to UvrB and Mfd, the existing population of UvrB is now required to turnover a greater number of UvrA molecules on undamaged DNA and at sites of GGR, in addition to TCR intermediates. This model predicts that Mfd and UvrA must form a TCR intermediate whose disassembly is contingent on the arrival of UvrB.

TCR is prioritized in cells after UV irradiation

Next, we set out to characterize the behaviour of the UvrA in response to DNA damage. UV irradiation leads to the formation of UV-induced lesions in the chromosome[39]. These in turn elicit the induction of the SOS response during which the expression of UvrA and UvrB are upregulated[40]. The elevated levels of UvrA promote rapid removal of UV lesions from the DNA. To quantify this process in real time, we set out to monitor the relative abundance of UvrA in cells following UV irradiation.

Time-lapse experiments on UV-irradiated *uvrA-YPet* allowed us to monitor the cellular fluorescence of tagged UvrA as a function of time. We immobilized *uvrA-YPet* cells in a flow cell with a quartz window and delivered a dose of 20 Jm^{-2} of damaging 254-nm UV light (Fig. 5a). This was followed by acquiring a single snapshot upon laser illumination with 514-nm light, every five minutes for three hours. Quantification of cellular fluorescence intensities revealed that the integrated fluorescence intensities of single *uvrA-YPet* cells increase 30 minutes after UV exposure, consistent with the rapid deregulation of the SOS inducible *uvrA* promoter (Fig. 5b)[41, 42].

Since UV-induced lesions are a substrate for UvrAB (reviewed in ref. [1]), we then set out to measure the lifetime of UvrA in UV-irradiated cells. To that end, we irradiated TCR-deficient cells (*uvrA-YPet* Δ*mfd*) with a pulse of 254-nm UV light delivered *in situ*. This was followed by interval imaging in four rounds, each lasting 25 minutes. Analysis of the complete data set revealed binding kinetics of UvrA-YPet corresponding to a short-lived species with a lifetime ($\tau_{UvrA|\ \Delta mfd,\ UV\ fast}$) of 1.6 ± 0.1 s (77 ± 3%) and a long-lived species of UvrA corresponding to a lifetime of ($\tau_{UvrA|\ \Delta mfd,\ UV\ slow}$) 13.1 ± 0.6 s (23 ± 2%) (Fig. 5c, and Supplementary Fig. 4). Strikingly the lifetime of the slowly dissociating species was larger than that detected in the absence of exogeneous DNA damage (8.7 s).

Seeking an explanation for the increase in binding lifetime of UvrA-YPet following UV exposure, we wondered if the longer lifetime of UvrA detected in these experiments represented temporally averaged measurements. Since each set of interval measurements lasted 25 min, we proceeded to disaggregate each data set into the four constitutive 25-min intervals after UV exposure. Analysis of the resulting data from each time window revealed that the measured lifetime of UvrA in GGR changes as a function of the experimental timeline after the UV pulse (Fig. 5c, and Supplementary Fig. 4). Indeed, in the first 25 minutes, the lifetime of UvrA (9.6 ± 1 s) matched that measured in the absence of DNA damage (8.7 ± 0.4 s). This lifetime increased to a maximum of 15.3 ± 2 s in the 50-75 minute time window, finally plateauing to 15 ± 4 s in the 75-100 minute time window after UV exposure.

There are two main takeaways from these experiments. First, the lifetime of short-lived UvrA does not change upon UV exposure, and is identical to that measured in the absence of any exogenous DNA damage. We therefore conclude that this species is involved in binding undamaged DNA. Second, since

the lifetime of long-lived UvrA changes upon UV exposure, we conclude that this species is engaged in DNA repair.

The lifetime of Mfd is identical to the long lifetime of UvrA during the SOS response

Next, we repeated the interval imaging experiments on wild-type cells (*uvrA-YPet*) following exposure to a 20 Jm^{-2} pulse of 254-nm UV light provided *in situ*. In this case, UvrA-YPet exhibited two kinetic populations after UV-exposure, a short-lived population with a lifetime of 1.4 ± 0.1 s (72 ± 5 %) and a second, longer lived population with a lifetime of 10.0 ± 0.4 s (28 ± 5%) (Fig. 5d, and Supplementary Fig. 5). As before, we disaggregated each data set into the four constitutive 25-min intervals after UV exposure. In contrast to TCR-deficient cells, the measured lifetime of UvrA stayed relatively constant in wild-type cells remaining low (8.4 ± 0.6 s) in the 75-100 minute time window after UV exposure. These data indicate that UvrA is turned over faster in an Mfd-dependent manner.

We followed these studies with an investigation of the binding lifetimes of Mfd. In the absence of exogeneous DNA damage, the lifetime of Mfd is 18 s[10]. Interval imaging of Mfd-YPet in *mfd-YPet* cells exposed to UV light revealed that the lifetime of Mfd-YPet dropped during the course of the SOS response, leading to an average lifetime ($\tau_{Mfd|UV}$) of 12 s (Fig. 5d, and Supplementary Fig. 6). Strikingly, the binding lifetime of Mfd mirrored that of UvrA in wild-type cells in the time window from 25-100 min after UV, providing further evidence in support of an Mfd-UvrA complex in cells.

UvrA forms a highly stable complex on DNA in the absence of UvrB

Two lines of evidence suggest that Mfd interacts with UvrA in cells. First, under conditions where excess UvrA is present relative to UvrB, a slowly dissociating species of UvrA can be identified that is sensitive to rifampicin treatment. Second, TCR-proficient cells exhibit rapid turnover of UvrA in the SOS response, unlike TCR-deficient cells where the lifetime of UvrA on DNA grows longer upon UV treatment. We therefore directly tested whether Mfd and UvrA interact in cells. Attempts at co-localization using spectrally separated probes, YPet and PAmCherry, were limited by the poor expression of Mfd-PAmCherry and UvrA-PAmCherry in cells under our standard growth conditions (Supplementary Note 1 and Supplementary Fig. 7). Instead, we opted to measure the binding lifetime of UvrA in cells lacking UvrB. Under these conditions, UvrA can form surveillance complexes ($UvrA_2$) and interact with Mfd. Interval imaging of UvrA-YPet in cells lacking UvrB (*uvrA-YPet* Δ*uvrB*) revealed a single long-lived UvrA species with a lifetime ($\tau_{UvrA|\Delta uvrB}$) of 97 ± 18 s (Fig. 5e, Supplementary Fig. 8). Since UvrA alone binds DNA with a lifetime of 24 s, this highly stable species must reflect interactions with Mfd. Considering that UvrA can interact with Mfd and arrest its translocation *in vitro* [11], we

propose that this slowly dissociating species reflects the arrested Mfd-UvrA complex in cells lacking UvrB (Fig. 5e).

Discussion

UvrA is the central player in NER since it performs critical functions in both GGR and TCR: First, it recognizes DNA damage as $UvrA_2$ or $UvrA_2B_{(2)}$ and loads UvrB in GGR and second, it stimulates TCR by interacting with Mfd. In cells, UvrA exhibits foci with residence times ranging from a few hundred milliseconds, to tens of seconds. To identify the lifetimes of the different populations of UvrA engaged in various repair functions, we applied an interval imaging strategy that enabled us to de-convolute binding kinetics from photobleaching kinetics. This combination of chemical and genetic tools enabled us to characterize the properties of UvrA in its various roles in nucleotide excision repair in cells.

First, using repair-deficient mutant UvrA, we identified that UvrA is long-lived in the absence of Mfd and UvrB. In the presence of UvrB, we found that UvrA dissociated faster, consistent with previous studies demonstrating that UvrB promotes the dissociation of UvrA *in vitro*. The short-lived population of UvrA(B) with a lifetime of ~2 s on DNA corresponds to UvrA(B) engaged in damage search.

In the absence of exogenous DNA damage, we also detected a lifetime of 8.7 s corresponding to the UvrA-mediated UvrB loading reaction in cells in GGR. In the presence of both UvrB and Mfd, we detected a long-lived species with a lifetime of 12 s. This observation was also reproduced in cells exposed to UV light. Further, the β-hairpin mutant UvrB that is poorly loaded on DNA stabilized UvrA on DNA. Together, these observations lead us to conclude that the long-lived species of UvrA conduct the UvrB loading reaction.

Cells lacking UvrB exhibited UvrA-YPet foci that were five-fold longer lived compared to UvrA-YPet in cells lacking both Mfd and UvrB, suggesting that UvrA forms a highly stable complex with Mfd. However, in the presence of UvrB, the DNA binding kinetics of UvrA in TCR could only be distinguished from UvrA in GGR under certain conditions. When UvrA-YPet concentrations are almost eight-fold higher than those obtained in *uvrA-YPet* cells, a rif-sensitive population of UvrA, involved in TCR is readily detectable. This population of UvrA exhibits a lifetime of 19 s. Intriguingly this long-lived population is undetectable in *uvrA-YPet* cells where UvrA-YPet is present at a lower concentration. Instead, in cells expressing UvrA-YPet from the chromosomal locus, the measured lifetime of UvrA-YPet is significantly shorter (12 s), and treatment with rif produced a lifetime of 9.6 s that is comparable to that of UvrA-YPet in Δ*mfd* cells (8.7 s). Together these findings demonstrate that the rate limiting step for the release of UvrA from TCR intermediates is determined by UvrB (Fig. 5f). A striking implication from these studies is that the binding lifetime of UvrA in the context of its UvrB

loading function during TCR depends on the relative abundance of UvrB, since an increase in the [UvrA] relative to [UvrB] represents a condition where the [UvrB] becomes limiting. A prediction of this hypothesis is that elevated concentrations of UvrB would lead to an enhancement of the rate of TCR observed in our experiments.

In response to UV exposure, cells induce the SOS response during which the *uvrA* promoter is de-repressed early, leading to elevated concentrations of UvrA in cells. In TCR-deficient cells, we found that the lifetime of UvrA increases as a function of time after UV exposure. Since UvrB plays a role in dissociating UvrA from DNA, such a situation may arise when UvrB cannot efficiently locate $UvrA_2$ bound to DNA damage. This may be attributable to the increase in cell volume owing to cell filamentation, dilution of DNA damage due to continued DNA replication and presence of excess competitor undamaged DNA. The continued synthesis of DNA following UV irradiation leads to the generation of additional substrates that must be probed by UvrA, in effect sequestering UvrB to UvrA bound to undamaged DNA. This in turn could lead to a delay in the dissociation of UvrA bound to DNA damage, manifesting as a longer lifetime in our experiments.

Surprisingly, this delay in UvrA dissociation was not observed in the case of cells carrying Mfd. Instead, UvrA was rapidly turned over in TCR-proficient cells. Additionally, the data revealed that the lifetime of Mfd mirrored that of UvrA in wild-type cells after UV damage. The faster turnover of UvrA is therefore attributable to its participation in complexes with Mfd. Under conditions of elevated UvrA concentrations relative to UvrB, the longer lifetime of UvrA may correspond to a longer wait time associated with a lower population of available UvrB.

Finally, by demonstrating that the lifetime of UvrA in TCR is not shorter than that in GGR, our data suggest that the enhancement of the rate of repair in TCR vs. GGR measured in bulk is best explained by enhanced target search in TCR compared to GGR. This model has been previously proposed in the literature based on evidence from *in vitro* studies. In this model, stalled RNAP is recognized by Mfd, leading to the exposure of Mfd's UvrB-homology module (BHM) that in turn acts as an 'antenna' for UvrAB. Damage recognition by UvrAB would then follow initial recruitment to the site of the lesion. In contrast, target search during global genomic repair would comprise of repeated cycles of 3D diffusion of UvrA(B) to sites of undamaged DNA followed by subsequent turn-over of UvrA by UvrB until the damage surveillance complex stochastically encounters damaged DNA.

METHODS

Construction of strains and plasmids

Escherichia coli MG1655 *uvrA-YPet* was constructed using λ Red recombination as previously described for Mfd[10]. Sequence specified wild-type *uvrA* and *uvrA*(Δ131-250) geneblocks (including the native *uvrA* promoter) were ordered from IDT (Coralville, USA) and subcloned into pHH001[10] using standard molecular biology techniques. Plasmids were sequenced on both strands prior to use. Strain expressing mutant UvrB was created using CRISPR-Cas9 assisted λ Red recombination as previously described[43, 44] (see Supplementary Method).

Cell culture for imaging

Cells were imaged in quartz-top flow cells as described previously[10]. Cells were grown in 500 µL of EZ-rich defined media (Teknova, CA, US), supplemented with 0.2% (v/v) glucose in 2 mL microcentrifuge tubes at 30 °C. For experiments involving plasmid-expressed UvrA-YPet or UvrA(Δ131-250)-YPet, spectinomycin (50 µg per mL) was added to the growth media. Cells in early exponential phase were loaded in flow cells at 30 °C, followed by a constant supply of aerated EZ-rich defined media at a rate of 30 µL per min, using a syringe pump (Adelab Scientific, Australia).

Single-molecule live-cell imaging

Single-molecule fluorescence imaging was carried out with a custom-built microscope as previously described[10]. Briefly, the microscope comprised a Nikon Eclipse Ti body, a 1.49 NA 100x objective, a 514-nm Sapphire LP laser (Coherent) operating at a power density of 71 $W.cm^{-2}$, an ET535/30m emission filter (Chroma) and a 512 x 512 $pixel^2$ EM-CCD camera (either Photometrics Evolve or Andor iXon 897). The microscope operated in near-TIRF illumination[45] and was controlled using NIS-Elements (Nikon). PAmCherry-tagged proteins were imaged as described previously[10].

Fluorescence images were acquired in time-series format with 0.1-s frames. Each video acquisition contained two phases. The first phase aimed to lower background signal by continuous illuminating, causing most of the fluorophores to photo-bleach or to assume a dark state. The second phase (single-molecule phase) is when single molecules can be reliably tracked on a low background signal. In the second phase, consecutive frames were acquired continuously or with a delay time (τ_d).

Image analysis

Image analysis was performed in Fiji[46], using the Single Molecule Biophysics plugins (available at https://github.com/SingleMolecule/smb-plugins), and MATLAB. First, raw data were converted to TIF

format, following by background correction and image flattening as previously described[10]. Next, foci were detected in the reactivation phase by applying a discoidal average filter (inner radius of one pixel, outer radius of three pixels), then selecting pixels above the intensity threshold. Foci detected within 3-pixel radius (318 nm) in consecutive frames were considered to belong to the same binding event.

Interval imaging for dissociation kinetics measurements

Interval imaging was performed as described previously[10]. The photobleaching phase contained 50 continuous 0.1-s frames. In phase II, 100 0.1-s frames were collected with time-lapse time (τ_{tl}) ranging from τ_{tl} = (0.1, 0.2, 0.5, 1, 2, 4, 8, 10). In each experiment, videos with varying τ_d were acquired. Foci were detected using a relative intensity threshold of 7 or 8 above the background as appropriate. Depending on the construct being imaged, between 3-15 repeats of each experiment were collected for each strain. Cumulative residence time distribution of binding events detected in all data sets were generated for each interval.

The effective off-rate constant k_{eff}, contributively of the photobleaching rate k_b and the off-rate k_{off}, was obtained by fitting the cumulative residence time distribution to a single-exponential model. The corresponding $k_{eff}\tau_{tl}$ vs. τ_{tl} plot was obtained as described previously[10, 22], with the shaded error bar representing standard deviations of ten bootstrapped samples deriving from 80% of the complied binding events (custom-written MATLAB codes)[22]. In experiments involving rifampicin treatment, cells were incubated in growth media containing rifampicin (50 μg per mL) for 30 min in the flow cell prior to imaging.

Experiments involving UV irradiation

UV survival assays were performed as described previously[47]. UV irradiation was delivered *in situ* as described previously[47]. The UV flux was measured prior to UV irradiation, and the exposure time was adjusted to provide a dose of 20 Jm^{-2}. For experiments involving interval imagine following UV exposure, τ_{tl} = (0.1, 0.3, 1, 3, 10) values were used to minimize the time taken to complete one round of interval imaging.

ACKNOWLEDGEMENTS

H.G. acknowledges the University of Wollongong and the Faculty of Science, Medicine and Health for funding of the Andor iXon 897 used in this work. A.M. van Oijen would like to acknowledge support by the Australian Research Council (DP150100956 and FL140100027).

AUTHOR CONTRIBUTIONS

Construct creation: H.G. and H.N.H.; Data curation: H.G.; Data analysis: H.G. and H.N.H.; Software: H.N.H. and H.G.; Writing—Original draft: H.G.; Writing—review and editing: H.N.H., H.G. and A.M.v.O.; Conceptualization: H.G.; Supervision: H.G. and A.M.v.O.

Competing interests

The authors declare no competing interests.

Materials and Correspondence

Harshad Ghodke, Molecular Horizons and School of Chemistry and Molecular Bioscience, University of Wollongong, Wollongong, New South Wales, 2522, Australia

FIGURES

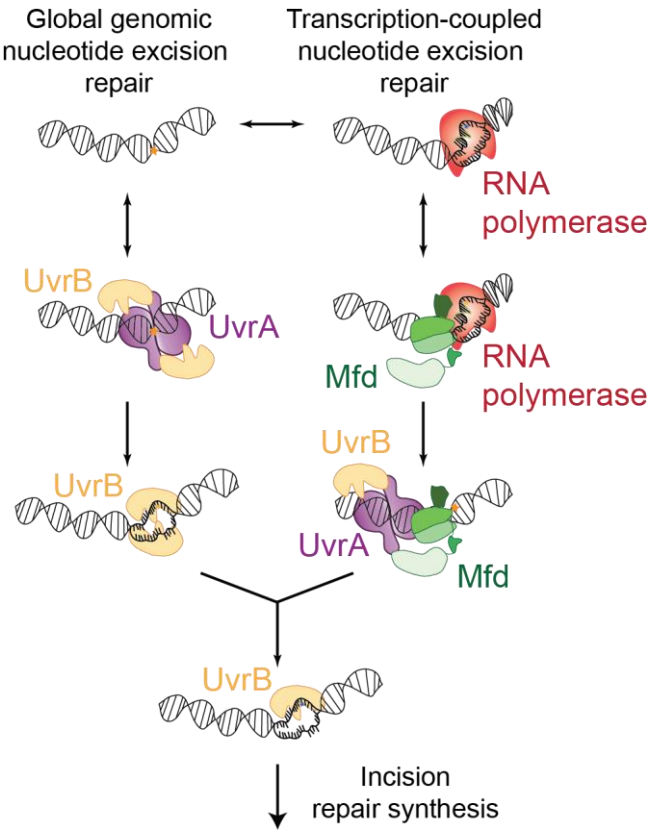

Figure 1: Nucleotide excision repair in *Escherichia coli*

Damage detection in nucleotide excision repair in *E. coli* proceeds via global damage surveillance executed by $UvrA_2(B)$, and RNA polymerase transcribing damaged template DNA. The UvrA dimer loads UvrB which verifies the presence of DNA damage in a strand-specific manner. Alternately, stalled elongation complexes at the site of DNA damage are rescued by the transcription repair coupling factor Mfd, which in turn recruits $UvrA_2(B)$ to the site of the stalled RNAP. This is followed by strand-specific loading of UvrB at the site of the lesion. Following damage verification by UvrB, a single-stranded patch of DNA containing the damage is incised by the UvrC endonuclease. This is followed by repair synthesis and ligation coordinated by UvrD, PolI and LigA.

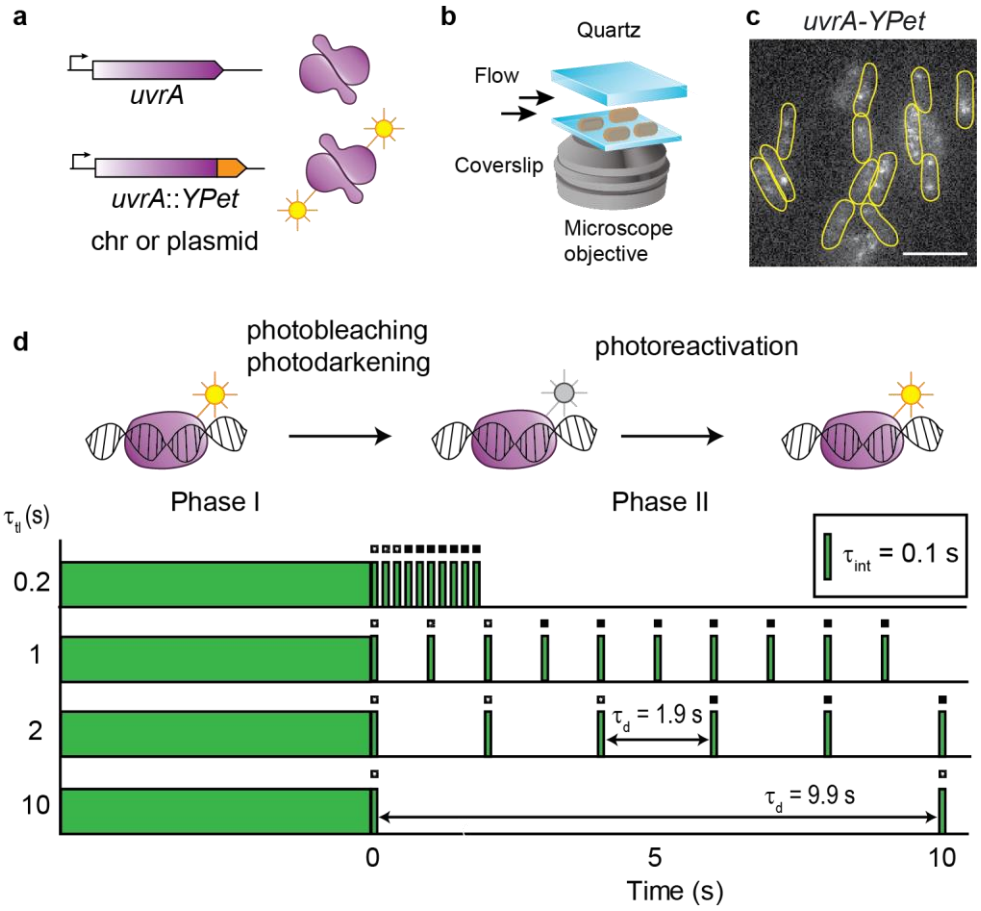

Figure 2: Construction of *uvrA-YPet* and imaging of UvrA-YPet

a. A chromosomal fusions of UvrA to the yellow fluorescent protein (YPet) under the native *uvrA* locus was created using λ Red recombination in MG1655 cells. In a second approach, the *uvrA-YPet* allele was expressed under the native *uvrA* promoter from a low-copy plasmid in Δ*uvrA* cells.

b. Cells expressing fluorescent UvrA-YPet were grown to early exponential phase and loaded in a flow cell. Cells were imaged under constant supply of aerated growth medium for several hours.

c. Fluorescence images of UvrA-YPet reveal a mixture of foci and diffuse cellular background signal. Scale bar represents 5 µm. Cell outlines are provided as a guide to the eye.

d. Schematic of interval imaging approach employed to measure the off rates of fluorescently tagged proteins in cells. Each acquisition is collected in two phases. In the first phase, fluorescent signal is bleached to enable observation of single fluorescent YPet molecules. In the second phase, a dark frame τ_d is introduced such that the time-lapse time $\tau_{tl} = \tau_d + \tau_{int}$, where τ_{int} is the integration time (100 ms). In this phase, the lifetimes of individual binding events of UvrA-YPet molecules are measured and combined to obtain a cumulative residence time distribution.

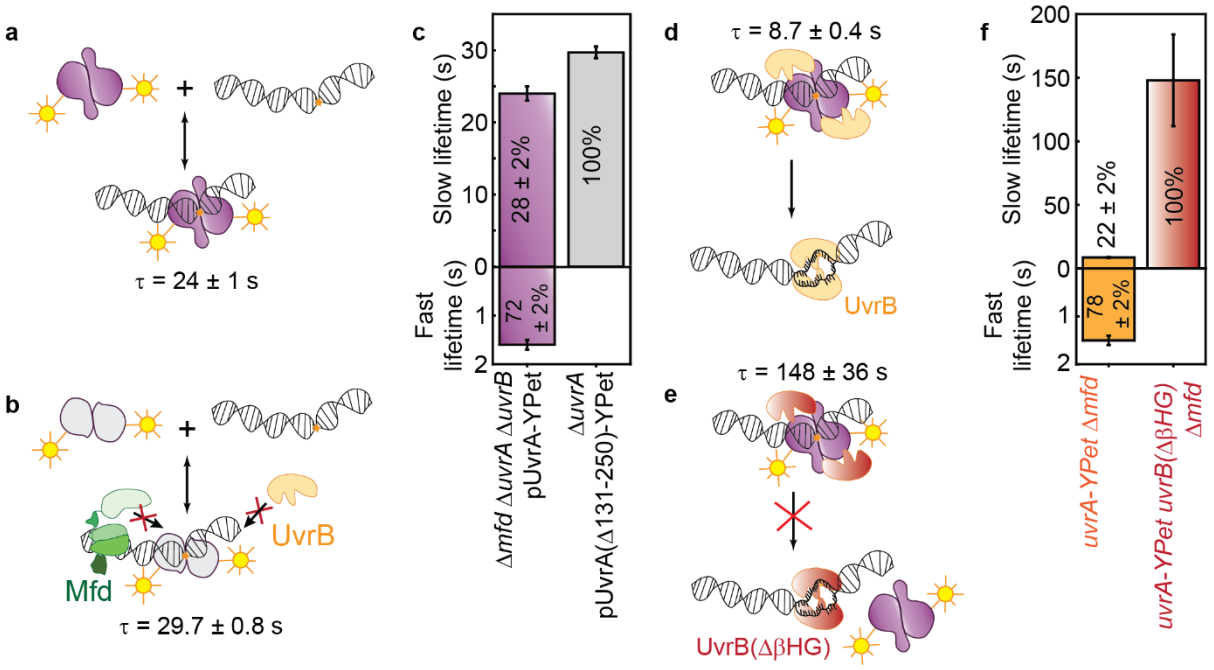

Figure 3: Kinetics of dissociation of UvrA-YPet in GGR

a. Kinetics of UvrA-YPet interactions with DNA can be detected in the absence of UvrB and Mfd, in Δ*uvrA* Δ*uvrB* Δ*mfd* cells expressing UvrA-YPet from plasmids.

b. Cartoon illustrates DNA binding by the mutant UvrA(Δ131-250)-YPet, which is defective in interacting with UvrB and Mfd.

c. Bar plots represent lifetimes of DNA-bound UvrA-YPet and mutant UvrA(Δ131-250)-YPet in the corresponding genetic background. Lifetimes were obtained from globally fitting the cumulative residence time distributions (CRTDs), with more than 3,000 counts each CRTD (see Supplementary Fig. 2a,c). Where two kinetic sub-populations are detected, the fast lifetime is displayed in the lower panel. Percentage represents the amplitude of kinetic sub-populations. Error bars are standard deviations from ten bootstrapped CRTDs.

d. Cartoon illustrates loading of UvrB by UvrA during global genomic repair.

e. Cartoon illustrates the complex formed by UvrA and the mutant UvrB(ΔβHG) that is deficient in loading reaction.

f. Bar plots represent lifetimes of DNA-bound UvrA-YPet in Δ*mfd* cells expressing either wild-type UvrB or mutant UvrB(ΔβHG). Lifetimes were obtained from globally fitting the CRTDs, with more than 1,000 counts each CRTD (see Supplementary Fig. 2e,g). Where two kinetic sub-populations are detected, the

fast lifetime is displayed in the lower panel. Percentage represents the amplitude of kinetic sub-populations. Error bars are standard deviations from ten bootstrapped CRTDs.

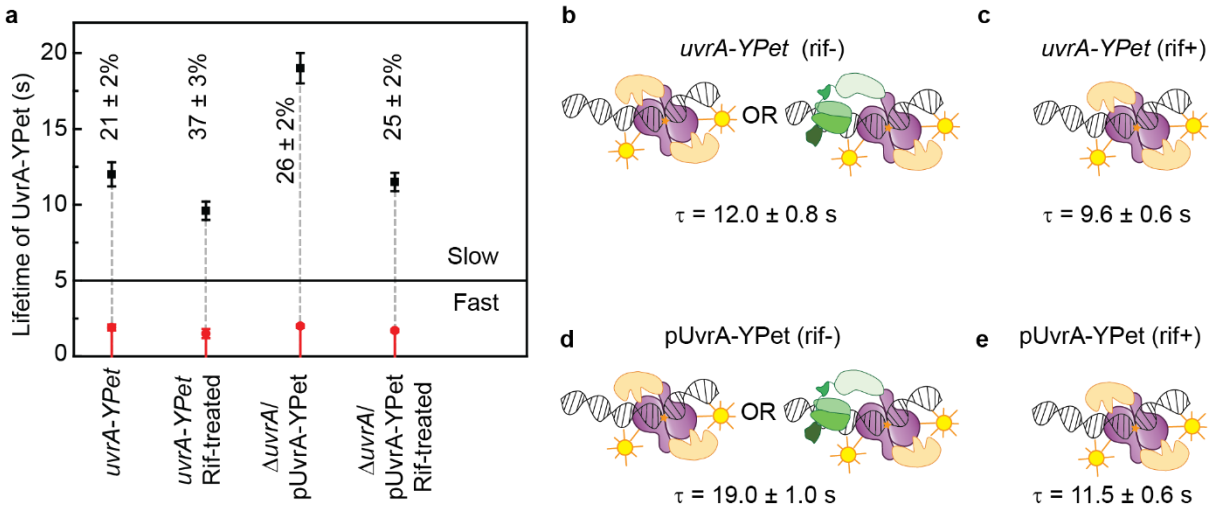

Figure 4: Dissociation kinetics of UvrA-YPet in wild-type cells

a. Lifetimes of UvrA-YPet in *uvrA-YPet* cells or Δ*uvrA*/pUvrA-YPet cells untreated or treated with rifampicin. Lifetimes were obtained from globally fitting the CRTDs, with 1,000-5,000 counts each CRTD (see Supplementary Fig. 3a,c,e,g). Black, the slow lifetime. Red, the fast lifetime. Percentages represent the amplitude of the slowly dissociating population. Error bars are standard deviations from ten bootstrapped CRTDs.

b. In the presence of UvrB and Mfd, UvrA-YPet in *uvrA-YPet* cells exhibited a slow lifetime of 12.0 ± 0.8 s, reflecting UvrA participating in both GGR and TCR.

c. Rifampicin treatment abolishes TCR, hence, UvrA-YPet is channelled towards GGR sub-pathway, with the slow lifetime was found to be 9.6 ± 0.6 s.

d. When UvrA-YPet concentration increased eight folds via the means of plasmid expression, the slow lifetime of UvrA-YPet in Δ*uvrA*/pUvrA-YPet cells was found to be 19 ± 1 s, longer than that of UvrA-YPet in *uvrA-YPet* cells (12 s).

e. Upon rifampicin treatment, the slow lifetime of UvrA-YPet in Δ*uvrA*/pUvrA-YPet cells reduced to 11.5 ± 0.6 s.

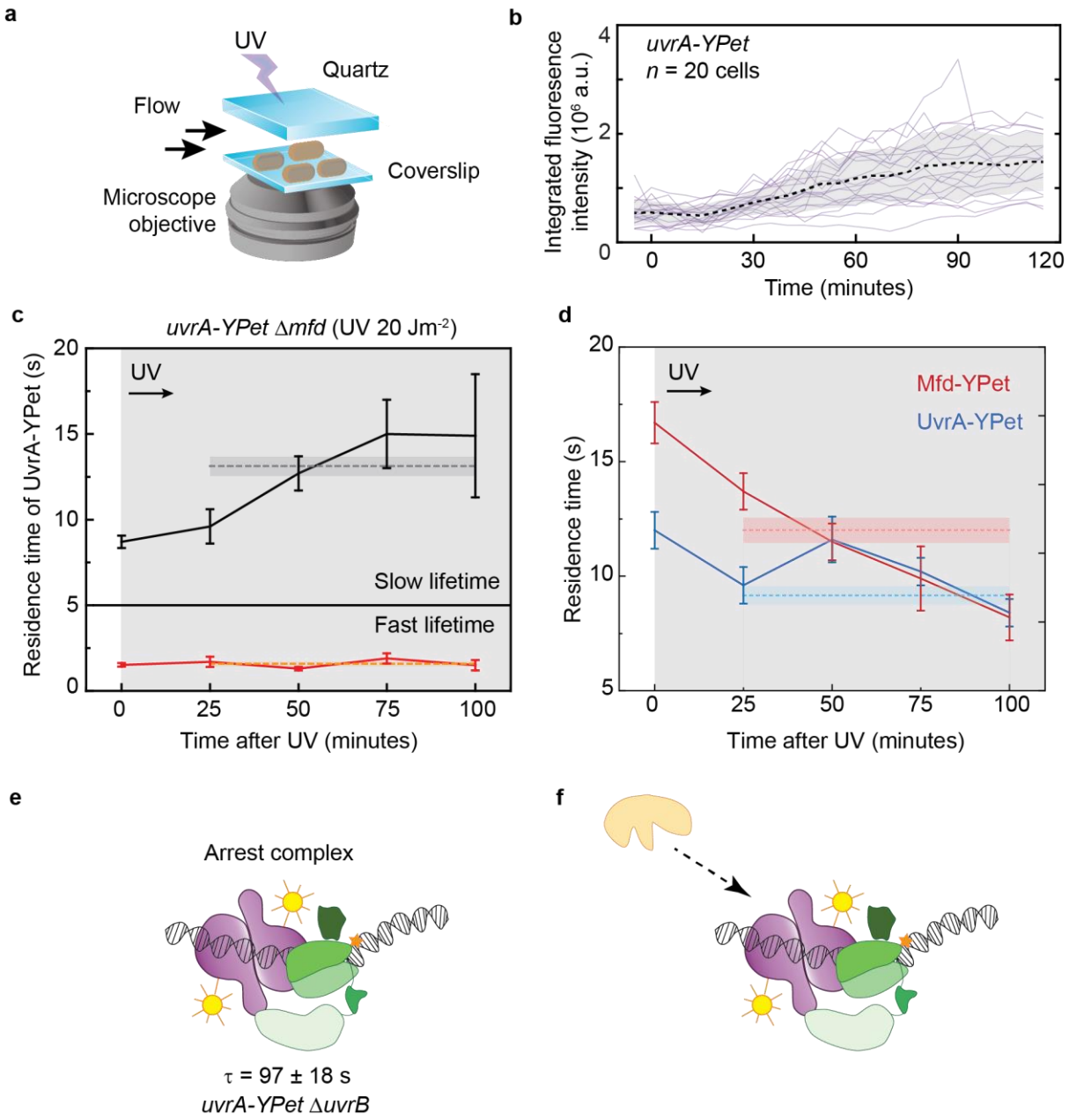

Figure 5: Lifetimes of DNA-bound UvrA and Mfd in response to UV irradiation

a. Experimental setup for introducing UV damage followed by interval imaging. A 20 Jm^{-2} dose of UV (254 nm) light is provided *via* a quartz window in the flow cell. This setup enables imaging of cells at 30 °C for several hours after UV.

b. Fluorescence intensity of single *uvrA-YPet* cells increases following exposure to UV light, indicating that expression of UvrA-YPet is upregulated in the SOS response.

c. Lifetimes of UvrA-YPet in TCR-deficient cells as a function of time following UV exposure. Lifetimes were obtained from globally fitting the CRTDs, with 400-2,000 counts each CRTD (see Supplementary Fig. 4a-d). Error bars are standard deviations from ten bootstrapped CRTDs. Lifetimes of the fast and

slowly dissociating sub-populations are shown in the lower and upper panels respectively. Dashed lines represent lifetimes obtained from aggregated CRTDs within 100 minutes following UV exposure. The lifetimes at t = 0 minutes represent those of UvrA-YPet in TCR-deficient cells during normal growth and are reproduced from Fig. 4a.

d. Lifetimes of UvrA-YPet in *uvrA-YPet* cells (blue) or Mfd-YPet in *mfd-YPet* cells (red) as a function of time following UV exposure. Lifetimes were obtained from globally fitting the CRTDs, with 250-2,000 counts each CRTD (see Supplementary Fig. 5a-d and Supplementary Fig. 6a-d). Error bars are standard deviations from ten bootstrapped CRTDs. Dash lines and error bands represent lifetimes and the corresponding standard deviations obtained from aggregated CRTDs within 100 minutes following UV exposure.

e. Cartoon illustrates the arrested Mfd-$UvrA_2$ (green and purple) complex observed with UvrA-YPet in cells lacking UvrB.

f. UvrB (orange) controls the release of UvrA (purple) from UvrA-Mfd (green) intermediates.

References

1. Van Houten B. Nucleotide excision repair in Escherichia coli. *Microbiol Rev* **54**, 18-51 (1990).

2. Kisker C, Kuper J, Van Houten B. Prokaryotic nucleotide excision repair. *Cold Spring Harb Perspect Biol* **5**, a012591 (2013).

3. Scharer OD. Nucleotide excision repair in eukaryotes. *Cold Spring Harb Perspect Biol* **5**, a012609 (2013).

4. Hanawalt PC, Spivak G. Transcription-coupled DNA repair: two decades of progress and surprises. *Nat Rev Mol Cell Biol* **9**, 958-970 (2008).

5. Xu J*, et al.* Structural basis for the initiation of eukaryotic transcription-coupled DNA repair. *Nature* **551**, 653-657 (2017).

6. Deaconescu AM, Darst SA. Crystallization and preliminary structure determination of Escherichia coli Mfd, the transcription-repair coupling factor. *Acta Crystallogr Sect F Struct Biol Cryst Commun* **61**, 1062-1064 (2005).

7. Selby CP, Sancar A. Molecular mechanism of transcription-repair coupling. *Science* **260**, 53-58 (1993).

8. Selby CP, Sancar A. Transcription-repair coupling and mutation frequency decline. *Journal of bacteriology* **175**, 7509-7514 (1993).

9. Selby CP, Witkin EM, Sancar A. Escherichia coli mfd mutant deficient in "mutation frequency decline" lacks strand-specific repair: in vitro complementation with purified coupling factor. *Proc Natl Acad Sci U S A* **88**, 11574-11578 (1991).

10. Ho HN, van Oijen AM, Ghodke H. The transcription-repair coupling factor Mfd associates with RNA polymerase in the absence of exogenous damage. *Nat Commun* **9**, 1570 (2018).

11. Fan J, Leroux-Coyau M, Savery NJ, Strick TR. Reconstruction of bacterial transcription-coupled repair at single-molecule resolution. *Nature* **536**, 234-237 (2016).

12. Sarker AH*, et al.* Recognition of RNA polymerase II and transcription bubbles by XPG, CSB, and TFIIH: insights for transcription-coupled repair and Cockayne Syndrome. *Mol Cell* **20**, 187-198 (2005).

13. Mellon I, Spivak G, Hanawalt PC. Selective removal of transcription-blocking DNA damage from the transcribed strand of the mammalian DHFR gene. *Cell* **51**, 241-249 (1987).

14. Sweder KS, Hanawalt PC. Preferential repair of cyclobutane pyrimidine dimers in the transcribed strand of a gene in yeast chromosomes and plasmids is dependent on transcription. *Proc Natl Acad Sci U S A* **89**, 10696-10700 (1992).

15. Ganesan AK, Hanawalt PC. Transcription-coupled nucleotide excision repair of a gene transcribed by bacteriophage T7 RNA polymerase in Escherichia coli. *DNA Repair (Amst)* **9**, 958-963 (2010).

16. Mellon I, Hanawalt PC. Induction of the Escherichia coli lactose operon selectively increases repair of its transcribed DNA strand. *Nature* **342**, 95-98 (1989).

17. Bohr VA, Smith CA, Okumoto DS, Hanawalt PC. DNA repair in an active gene: removal of pyrimidine dimers from the DHFR gene of CHO cells is much more efficient than in the genome overall. *Cell* **40**, 359-369 (1985).

18. Smerdon MJ, Thoma F. Site-specific DNA repair at the nucleosome level in a yeast minichromosome. *Cell* **61**, 675-684 (1990).

19. Howan K*, et al.* Initiation of transcription-coupled repair characterized at single-molecule resolution. *Nature* **490**, 431-434 (2012).

20. Manelyte L, Kim YI, Smith AJ, Smith RM, Savery NJ. Regulation and rate enhancement during transcription-coupled DNA repair. *Mol Cell* **40**, 714-724 (2010).

21. Stracy M*, et al.* Single-molecule imaging of UvrA and UvrB recruitment to DNA lesions in living Escherichia coli. *Nat Commun* **7**, 12568 (2016).

22. Ho HN, Zalami, D., Köhler, J., van Oijen, A.M., Ghodke, H. Identifying multiple kinetic populations of DNA binding proteins in live cells using single-molecule fluorescence imaging. *bioRxiv*, (2019).

23. Nguyen AW, Daugherty PS. Evolutionary optimization of fluorescent proteins for intracellular FRET. *Nat Biotechnol* **23**, 355-360 (2005).

24. Datsenko KA, Wanner BL. One-step inactivation of chromosomal genes in Escherichia coli K-12 using PCR products. *Proc Natl Acad Sci U S A* **97**, 6640-6645 (2000).

25. Kad NM, Wang H, Kennedy GG, Warshaw DM, Van Houten B. Collaborative dynamic DNA scanning by nucleotide excision repair proteins investigated by single- molecule imaging of quantum-dot-labeled proteins. *Mol Cell* **37**, 702-713 (2010).

26. Schmidt A*, et al.* The quantitative and condition-dependent Escherichia coli proteome. *Nat Biotechnol* **34**, 104-110 (2016).

27. Gebhardt JC*, et al.* Single-molecule imaging of transcription factor binding to DNA in live mammalian cells. *Nat Methods* **10**, 421-426 (2013).

28. Liao Y, Li Y, Schroeder JW, Simmons LA, Biteen JS. Single-Molecule DNA Polymerase Dynamics at a Bacterial Replisome in Live Cells. *Biophys J* **111**, 2562-2569 (2016).

29. Churchward G, Belin D, Nagamine Y. A pSC101-derived plasmid which shows no sequence homology to other commonly used cloning vectors. *Gene* **31**, 165-171 (1984).

30. Pakotiprapha D*, et al.* Crystal structure of Bacillus stearothermophilus UvrA provides insight into ATP-modulated dimerization, UvrB interaction, and DNA binding. *Mol Cell* **29**, 122-133 (2008).

31. Pakotiprapha D, Samuels M, Shen K, Hu JH, Jeruzalmi D. Structure and mechanism of the UvrA-UvrB DNA damage sensor. *Nat Struct Mol Biol* **19**, 291-298 (2012).

32. Deaconescu AM, Sevostyanova A, Artsimovitch I, Grigorieff N. Nucleotide excision repair (NER) machinery recruitment by the transcription-repair coupling factor involves unmasking of a conserved intramolecular interface. *Proc Natl Acad Sci U S A* **109**, 3353-3358 (2012).

33. Malta E, Moolenaar GF, Goosen N. Dynamics of the UvrABC nucleotide excision repair proteins analyzed by fluorescence resonance energy transfer. *Biochemistry* **46**, 9080-9088 (2007).

34. Orren DK, Sancar A. The (A)BC excinuclease of Escherichia coli has only the UvrB and UvrC subunits in the incision complex. *Proc Natl Acad Sci U S A* **86**, 5237-5241 (1989).

35. Lin JJ, Sancar A. (A)BC excinuclease: the Escherichia coli nucleotide excision repair enzyme. *Mol Microbiol* **6**, 2219-2224 (1992).

36. Skorvaga M, Theis K, Mandavilli BS, Kisker C, Van Houten B. The beta -hairpin motif of UvrB is essential for DNA binding, damage processing, and UvrC-mediated incisions. *J Biol Chem* **277**, 1553-1559 (2002).

37. Skorvaga M*, et al.* Identification of residues within UvrB that are important for efficient DNA binding and damage processing. *J Biol Chem* **279**, 51574-51580 (2004).

38. DellaVecchia MJ, Croteau DL, Skorvaga M, Dezhurov SV, Lavrik OI, Van Houten B. Analyzing the handoff of DNA from UvrA to UvrB utilizing DNA-protein photoaffinity labeling. *J Biol Chem* **279**, 45245-45256 (2004).

39. Rastogi RP, Richa, Kumar A, Tyagi MB, Sinha RP. Molecular mechanisms of ultraviolet radiation-induced DNA damage and repair. *J Nucleic Acids* **2010**, 592980 (2010).

40. Crowley DJ, Hanawalt PC. Induction of the SOS Response Increases the Efficiency of Global Nucleotide Excision Repair of Cyclobutane Pyrimidine Dimers, but Not 6-4 Photoproducts, in UV-Irradiated Escherichia coli. *Journal of Bacteriology* **180**, 3345-3352 (1998).

41. Courcelle J, Khodursky A, Peter B, Brown PO, Hanawalt PC. Comparative gene expression profiles following UV exposure in wild-type and SOS-deficient Escherichia coli. *Genetics* **158**, 41-64 (2001).

42. Kenyon CJ, Walker GC. Expression of the E. coli uvrA gene is inducible. *Nature* **289**, 808-810 (1981).

43. Jiang W, Bikard D, Cox D, Zhang F, Marraffini LA. RNA-guided editing of bacterial genomes using CRISPR-Cas systems. *Nat Biotechnol* **31**, 233-239 (2013).

44. Pyne ME, Moo-Young M, Chung DA, Chou CP. Coupling the CRISPR/Cas9 System with Lambda Red Recombineering Enables Simplified Chromosomal Gene Replacement in Escherichia coli. *Appl Environ Microbiol* **81**, 5103-5114 (2015).

45. Tokunaga M, Imamoto N, Sakata-Sogawa K. Highly inclined thin illumination enables clear single-molecule imaging in cells. *Nat Methods* **5**, 159-161 (2008).

46. Schindelin J*, et al.* Fiji: an open-source platform for biological-image analysis. *Nat Methods* **9**, 676-682 (2012).

47. Ghodke H, Paudel, B., Lewis, J. S., Jergic, S., Gopal, K., Romero, Z. J., Wood, E. A., Woodgate, R., Cox, M. M., van Oijen, A. M. Spatial and temporal organization of RecA in the Escherichia coli DNA-damage response. *bioRxiv*, (2018).